Parameter Evaluation of Permanent Magnet Synchronous Machines with Tooth Coil Windings using the Frozen Permeabilities Method with the Finite Element Analyses

Erich Schmidt, *Member*, *IEEE*, Marko Sušić
Institute of Energy Systems and Electric Drives, Vienna University of Technology, Vienna, Austria

Abstract – **Permanent magnet synchronous machines with fractional slot stator windings using the tooth coil technology require detailed investigations on the electromagnetic parameters due to a very low number of slots per pole and phase. Finite element analyses can provide many results but a subsequent application of the frozen permeabilities method allows for a more detailed discussion of effects caused by both permanent magnets and armature stator currents in conjunction with angular rotor position and also different saturation levels. In particular, these detailed analyses are required for high performance electrical drive systems which operate under very fast changing load conditions and additionally run in deep field weakening ranges.**

Keywords – **Two-axes inductances, Frozen permeabilities, Reluctance machine, Permanent magnet machine, Synchronous machine, Finite element analysis**

I. Introduction

The electromagnetic torque of permanent magnet synchronous machines arises from the interaction of the linkage flux caused by the permanent magnets mounted in the rotor and the magneto motive force of the armature currents in the stator. During the design process of such machines, it is desirable to know the individual contributions from permanent magnets and stator currents in detail [1], [2]. This gains in significance when such machines are equipped with fractional slot stator windings using tooth coil technology due to their increased torque capability [3]–[5]. In these cases, the number of slots per pole and phase is in the range of $1/4 \leq q \leq 1/2$. Thus, super- and sub-harmonics of the magneto motive force of the armature currents influence the machine characteristics more significantly. Due to the very low number of slots per pole and phase, cross-coupling effects between the direct and quadrature axes have to be considered, too.

The utilization of the frozen permeabilities method within the finite element analyses allows for these detailed investigations [6]–[9]. Moreover, this method provides a straight-forward strategy for an evaluation of the apparent inductances of such machines in dependence on the stator currents and the rotor position.

By using the frozen permeabilities method, the paper discusses evaluation of the linkage flux of the permanent magnets and the apparent two-axes inductances in dependence on the load condition. Subsequently, the evolved electromagnetic torques obtained from linkage flux and inductances as well as directly from the non-linear finite element analysis are compared. Further, the individual components of the electromagnetic torque produced from either the permanent magnets and the armature currents as well as the zero sequence currents in case of the delta-connected stator winding are shown in detail. In order to validate the numerical results, the electromagnetic torque is compared with measurement results of a prototype machine.

II. Machine Design and Finite Element Model

Fig. 1 depicts the investigated permanent magnet synchronous machine with an external rotor and a single-layer fractional slot winding with tooth coils [10], [11].

As shown in Fig. 1, the smallest necessary section of the entire machine for the finite element model consists of only five poles representing a half of a base winding. To

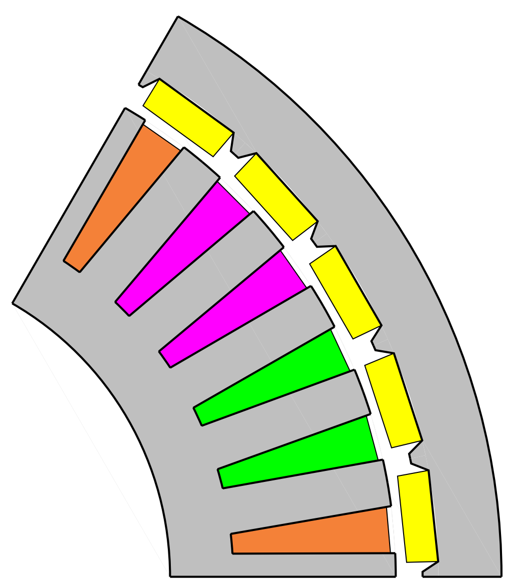

Fig. 1: Cross section of the external rotor permanent magnet synchronous machine with 30 poles and 36 slots

reflect the required periodicity of the magnetic field with the unknown degrees of freedom of the magnetic vector potential, anti-periodic boundary conditions are utilized at the boundaries being five pole pitches apart. For an application of the sliding surface method, stator and rotor model parts are meshed with an equidistant discretization in circumferential direction along the sliding surface interface within the air-gap [12]–[15].

For an utilization of the frozen permeabilities method, the various analyses are carried out in two steps [6]–[9]. First, non-linear solutions with various excitations and angular rotor positions are performed. With each of these results, the permeabilities of the non-linear finite elements are preserved for subsequent linear analyses which utilize the various excitations independently of each other.

III. Space Vector Calculus

In the dq rotor fixed reference frame, the normalized stator current and stator flux space vectors are given by

$$\underline{i}_{S,dq} = i_S \, \mathrm{e}^{j\beta} \;= i_{Sd} + j \, i_{Sq} \;\; , \tag{1}$$

$$\underline{\psi}_{S,dq} = \psi_S \, \mathrm{e}^{j\vartheta} = \psi_{Sd} + j \, \psi_{Sq} \;\; . \tag{2}$$

Therein, i_S,ψ_S represent the magnitudes of stator current and stator flux, β,ϑ denote stator current angle and stator flux angle, respectively. By using direct and quadrature axis inductances l_{dd},l_{qq} and cross-coupling inductances $l_{dq} = l_{qd}$ [16], the components of the stator linkage flux can be written as

$$\psi_{Sd} = l_{dd} \, i_{Sd} + l_{dq} \, i_{Sq} + \psi_{Md} \;\; , \tag{3a}$$

$$\psi_{Sq} = l_{qd} \, i_{Sd} + l_{qq} \, i_{Sq} + \psi_{Mq} \;\; , \tag{3b}$$

wherein ψ_{Md},ψ_{Mq} denote the linkage flux from the permanent magnets. Due to the cross-coupling between the axes, the permanent magnets solely arranged in direct axis generate a linkage flux in dependence on load and angular rotor position in both directions.

Consequently, the normalized electromagnetic torque follows from

$$\begin{aligned} t_i &= -\frac{3}{2} \, \mathrm{Im}\Big(\underline{i}^{*}_{S,dq} \, \underline{\psi}_{S,dq} \Big) = \frac{3}{2} \, \Big(\psi_{Sd} \, i_{Sq} - \psi_{Sq} \, i_{Sd} \Big) \\ &= \frac{3}{2} \, i_S \, \Big(\psi_{Md} \, \sin\beta - \psi_{Mq} \, \cos\beta \Big) \\ &+ \frac{3}{2} \, i_S^2 \, \Big(\frac{l_{dd} - l_{qq}}{2} \, \sin 2\beta - \frac{l_{dq} + l_{qd}}{2} \, \cos 2\beta \Big) \;\; . \end{aligned} \tag{4}$$

In order to inject the stator currents in the $\alpha\beta$ stator fixed reference frame of the finite element model, the stator current and stator flux space vectors are transformed as given by

$$\underline{i}_{S,\alpha\beta} = \underline{i}_{S,dq} \, e^{\jmath\gamma} \;\; , \tag{5}$$

$$\underline{\psi}_{S,\alpha\beta} = \underline{\psi}_{S,dq} \, e^{\jmath\gamma} \;\; , \tag{6}$$

where γ denotes the electric angular rotor position. In case of a Y-connected stator winding, any zero sequence stator currents i_0 are impossible. Thus, the stator currents are directly deduced as the projections onto the three stator axes. On the other hand in case of a Δ-connected stator winding, the zero sequence current i_0 must be used additionally. It is determined iteratively for each angular rotor position with all operating conditions according to the vanishing sum $\psi_{S1} + \psi_{S2} + \psi_{S3} = 0$ of the linkage fluxes of the three phases [10], [11].

IV. Analysis Results

A. Flux Linkages

Fig. 2 and Fig. 3 show the linkage flux within the stator winding caused by the permanent magnets in dependence on stator current magnitude and angle obtained from the frozen permeabilities method for the Y- and Δ-connected stator winding, respectively. Consequently, the different saturation in dependence on the current load significantly influences the linkage flux of the permanent magnets. In particular, positive direct currents noticeably decrease this linkage flux. On the other hand, due to the cross-coupling of the axes, there are appreciable portions of the linkage flux in quadrature axis particularly with high quadrature currents.

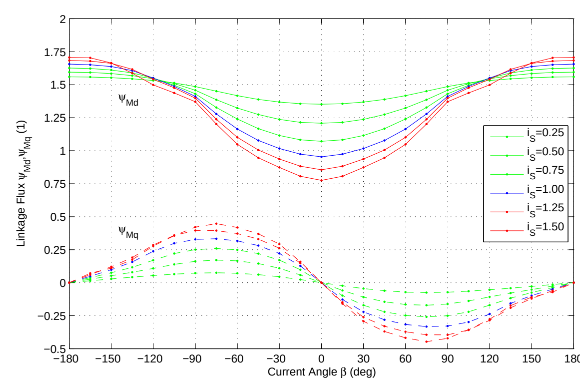

Fig. 2: Linkage flux of the permanent magnets versus current magnitude and angle, Y-connected stator winding

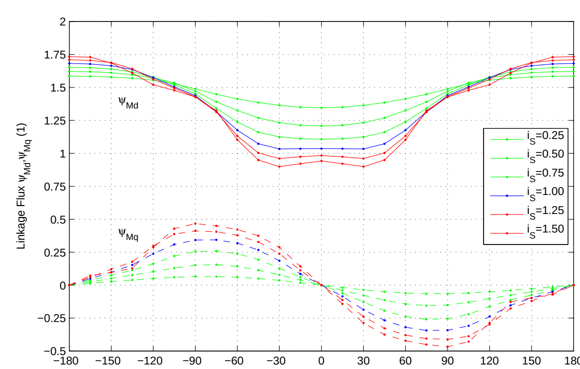

Fig. 3: Linkage flux of the permanent magnets versus current magnitude and angle, Δ-connected stator winding

B. Inductances

Fig. 4, Fig. 5, Fig. 6 and Fig. 7, Fig. 8, Fig. 9 depict the apparent inductances in dependence on stator current magnitude and angle obtained from the frozen permeabilities method for the Y- and Δ-connected stator winding, respectively. Obviously, both connections of the stator winding result in an inverse-saliency behaviour with $l_{dd} < l_{qq}$ for most current excitations with an exception of those with current angles nearby $\beta = \pm\pi/2$. The most significant difference between Y- and Δ-connection arises with the inductance l_{qq} with current angles nearby $\beta = 0$. With these excitations, the saturation along the direct axis is strongly enforced resulting in very high zero-sequence currents.

It has be mentioned, that in particular the apparent two-axes inductances l_{dd},l_{qq} are significantly different from the differential two-axes inductances as published in [11] which are in the range of $1.20 \geq l_{dd} \geq 0.2$ and $1.20 \geq l_{dd} \geq 0.4$. Only the differential cross-coupling inductances are in the same range as the apparent cross-coupling inductances.

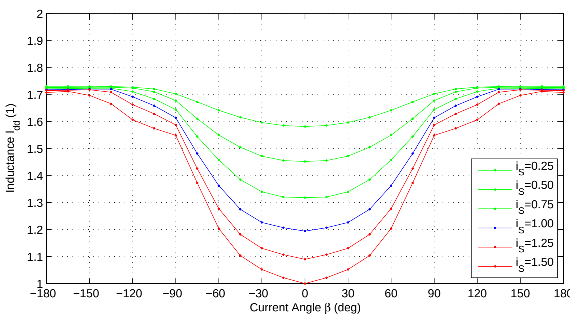

Fig. 4: Inductance l_{dd} versus current magnitude and angle, Y-connected stator winding

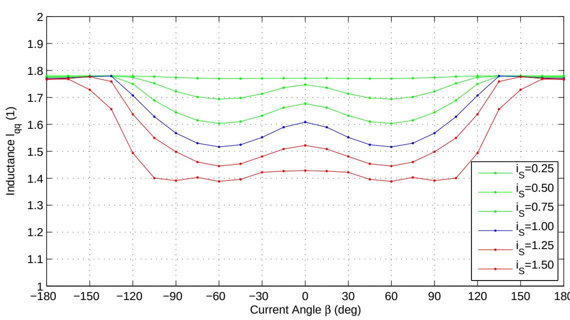

Fig. 5: Inductance l_{qq} versus current magnitude and angle, Y-connected stator winding

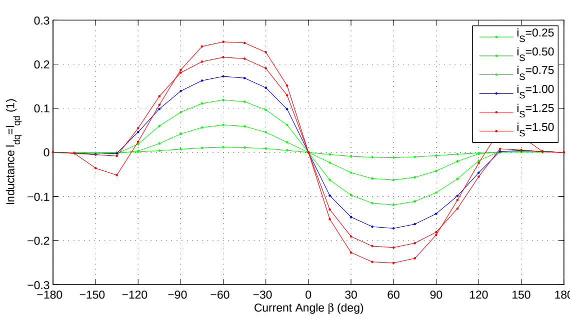

Fig. 6: Inductance $l_{dq} = l_{qd}$ versus current magnitude and angle, Y-connected stator winding

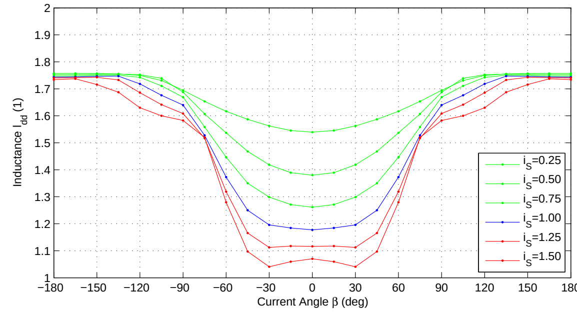

Fig. 7: Inductance l_{dd} versus current magnitude and angle, Δ-connected stator winding

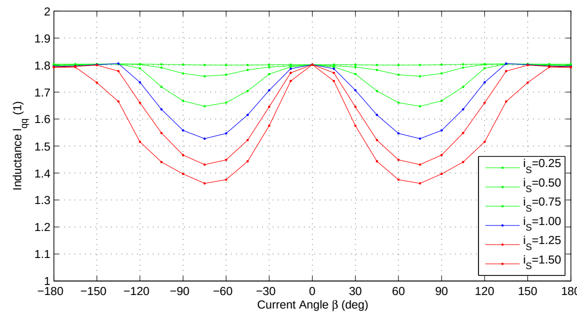

Fig. 8: Inductance l_{qq} versus current magnitude and angle, Δ-connected stator winding

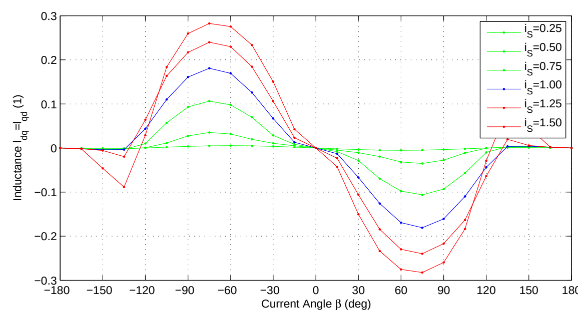

Fig. 9: Inductance $l_{dq} = l_{qd}$ versus current magnitude and angle, Δ-connected stator winding

C. Electromagnetic Torque

Fig. 10 and Fig. 11 show the contour maps for a constant electromagnetic torque. These current trajectories confirm an inverse-saliency behaviour with a saliency ratio l_{dd}/l_{qq} of the apparent two-axes inductances slightly less than one. On the other hand, the saliency ratio l_{dd}/l_{qq} of the apparent two-axes inductances changes to values slightly greater than one in the deep field weakening range. This is caused by a desaturation mainly with the direct axis with these operational conditions.

Fig. 12 and Fig. 13 show a comparison of the electromagnetic torque obtained directly from the non-linear analyses and those values evaluated using the two-axes inductances without and with cross-coupling terms with rated current and both winding connections. Obviously, an inclusion of the cross-coupling inductances describes

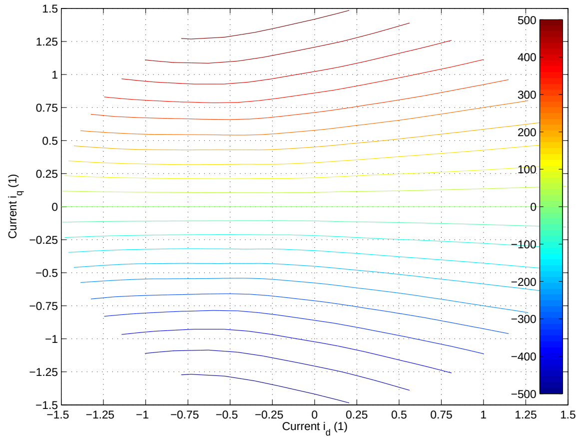

Fig. 10: Contour map of torque t_i versus stator current components i_d,i_q, Y-connected stator winding

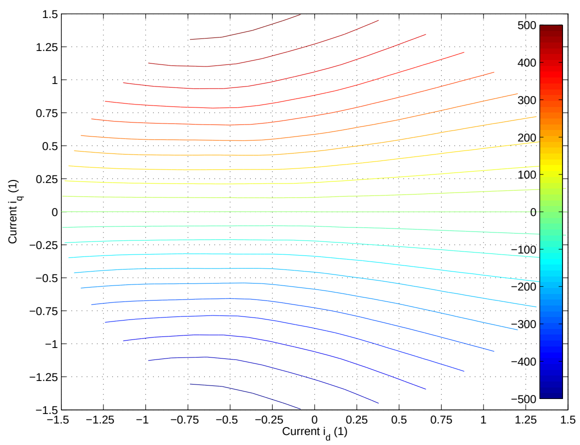

Fig. 11: Contour map of torque t_i versus stator current components i_d,i_q, Δ-connected stator winding

the inverse-saliency behaviour of the machine much better. The torque values evaluated from the two-axes apparent inductances represent the portion generated by the fundamental harmonics and cover approximately 80% of the total torque.

Fig. 14 and Fig. 15 depict the total electromagnetic torque obtained directly as well as the various components obtained from the frozen permeabilities method with rated quadrature axis current and both winding connections. With the Y-connected stator winding, the Maxwell stress tensor method yields four portions, the cogging torque of the permanent magnets denoted as $\mathrm{B_{rM}B_{pM}}$, the reluctance torque of the stator currents denoted as $\mathrm{B_{rI}B_{pI}}$ and the most significant two components arising from radial and azimuthal flux density components of permanent magnets and stator currents denoted as $\mathrm{B_{rM}B_{pI}}$ and $\mathrm{B_{rI}B_{pM}}$. With the Δ-connected stator winding, there are additionally the portion of the zero sequence current denoted as $\mathrm{B_{r0}B_{p0}}$ and the respective four cross-coupling portions denoted as $\mathrm{B_{rM}B_{p0}}$, $\mathrm{B_{rI}B_{p0}}$, $\mathrm{B_{r0}B_{pM}}$ and $\mathrm{B_{r0}B_{pI}}$. With both winding connections, the portion of the stator currents $\mathrm{B_{rI}B_{pI}}$ confirms a saliency ratio l_{dd}/l_{qq} slightly different from one. On the other hand, the portion of the permanent magnets $\mathrm{B_{rM}B_{pM}}$ always has the opposite sign of the total torque.

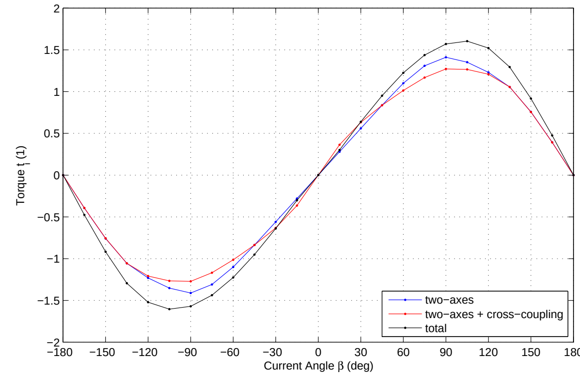

Fig. 12: Total torque and torque components from two-axes without and with cross-coupling inductances with rated current versus current angle, Y-connected stator winding

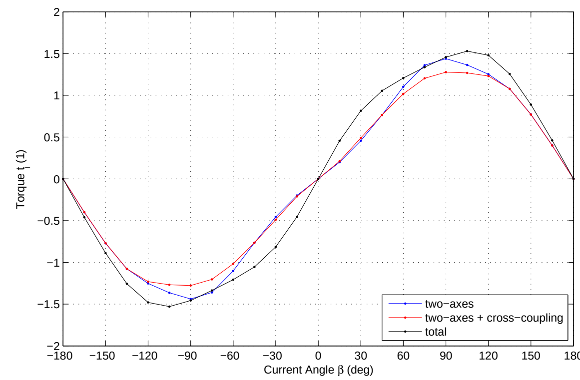

Fig. 13: Total torque and torque components from two-axes without and with cross-coupling inductances with rated current versus current angle, Δ-connected stator winding

D. Comparison with Measurements

Fig. 16 depicts the load torque in dependence on the quadrature axis current. The numerical results are shown for both Y- and Δ-connected stator windings while the measurement results are obtained from the initial design with a Δ-connected stator winding. There is a good agreement with stator currents in the range up to rated current loads but increasing deviations with higher current loads. They arise from stray field portions in the axial direction in particular with the permanent magnets of the rotor.

V. Conclusion

The paper discusses the application of the frozen permeabilities method for an evaluation of the apparent inductances and the subsequent analysis of the electromagnetic torque of an external rotor permanent magnet synchronous machine equipped with a fractional slot stator winding with concentrated tooth coils. Throughout all these calculations, both Y- and Δ-connected stator windings are concerned.

It is shown that apparent and differential inductances cannot be compared and have to be treated separately. While the latter ones are significant for in particular a sensorless control of such machines, the first ones are

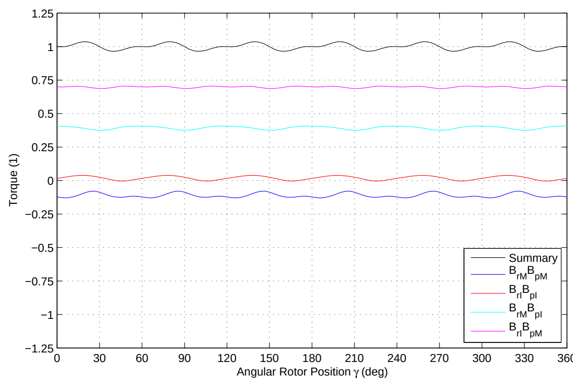

Fig. 14: Total electromagnetic torque and torque components with rated quadrature current, reference value of 364.5 Nm, Y-connected stator winding

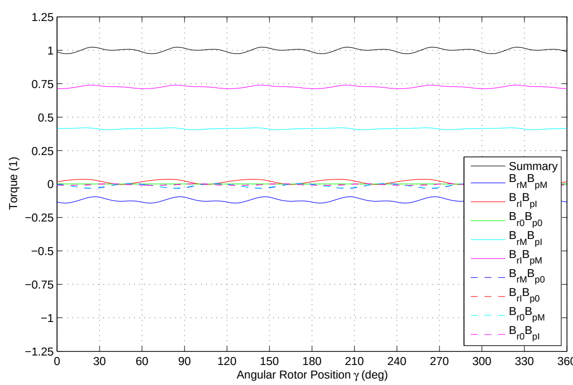

Fig. 15: Total electromagnetic torque and torque components with rated quadrature current, reference value of 353.3 Nm, Δ-connected stator winding

more interesting in design and optimization of the machine geometry. Further, a comparison of the torque obtained directly from the non-linear analyses is carried out with those torque values arising from the apparent two-axes inductances without and with cross-coupling inductances. On the other hand, the frozen permeabilities method also allows for a distinct treatment of the various portions within the evolved torque caused by permanent magnets, armature currents as well as zero-sequence currents in case of Δ-connected stator windings. With such approaches, effects of super- and sub-harmonics caused by the fractional slot stator winding can be analyzed in an efficient way.

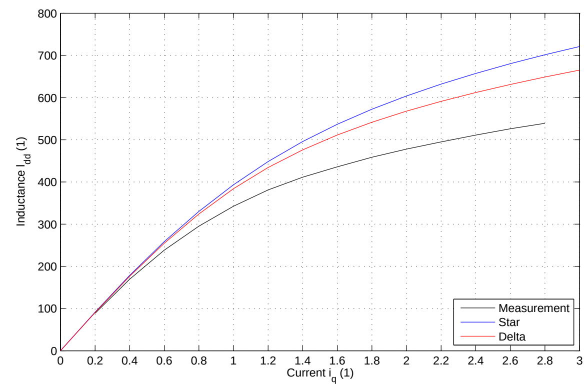

Fig. 16: Load torque, Y-connected and Δ-connected stator winding as well as measurement results [11]

References

[1] Bianchi N., Bolognani S., Chalmers B.J.: "Comparison of Different Synchronous Motors Drives for Flux Weakening Applications". *Proceedings of the 13th International Conference on Electric Machines, ICEM*, Instanbul (Turkey), 1998.

[2] Miller J.M., McClear P.J., Lang J.H.: "Starter-Alternator for Hybrid Electric Vehicle: Comparison of Induction and Variable Reluctance Machines and Drives". *Proceedings of the IEEE Industry Applications Society 33th Annual Meeting*, St.Louis (MO, USA), 1998.

[3] Huth G.: "Permanent Magnet Excited AC Servo Motors in Tooth Coil Technology". *IEEE Transactions on Energy Conversion*, Vol. 20, No. 2, June 2005.

[4] El-Refaie A.M., Shah M.R.: "Comparison of Induction Machine Performance with Distributed and Fractional Slot Concentrated Windings". *IEEE Industry Applications Society Annual Meeting, IAS*, Edmonton (AB, Canada), October 2008.

[5] El-Refaie A.M.: "Fractional Slot Concentrated Windings Synchronous Permanent Magnet Machines: Opportunities and Challenges". *IEEE Transactions on Industrial Electronics*, Vol. 57, No. 1, January 2010.

[6] Bianchi N.: *Electrical Machine Analysis Using Finite Elements*. CRC Press, Boca Raton (USA), 2005.

[7] Walker J.A., Dorrell D.G., Cossar C.: "Flux Linkage Calculation in Permanent Magnet Motors Using the Frozen Permeabilities Method". *IEEE Transactions on Magnetics*, Vol. 41, No. 10, October 2005.

[8] Tangudu J.K., Jahns T.M., El-Refaie A.M., Zhu Z.Q.: "Segregation of Torque Components in Fractional Slot Concentrated Winding Interior PM Machines Using Frozen Permeability". *Proceedings of the IEEE Energy Conversion Congress and Exposition, ECCE*, San Jose (CA, USA), September 2009.

[9] Xia Z.P., Zhu Z.Q., Wu L.J., Jewell G.W.: "Comparison of Radial Vibration Forces in 10-Pole/12-Slot Fractional Slot Surface Mounted and Interior Permanent Magnet Brushless AC Machines". *Proceedings of the 19th International Conference on Electrical Machines, ICEM*, Rome (Italy), 2010.

[10] Schmidt E., Susic M., Eilenberger A.: "Design Studies on a Permanent Magnet Synchronous Machine with Y- and Δ-connected Stator Winding". *IEEE Transactions on Magnetics*, Vol. 47, No. 05, May 2011.

[11] Schmidt E., Susic M.: "Finite Element Analyses of Permanent Magnet Synchronous Machines with Fractional Slot Tooth Coil Windings". *Elektrotechnik und Informationstechnik (e&i)*, Vol. 128, No. 03, 2011.

[12] Hameyer K., Belmans R.: *Numerical Modelling and Design of Electrical Machines and Devices*. WIT Press, Southampton (UK), 1999.

[13] Bastos J.P.A., Sadowski N.: *Electromagnetic Modeling by Finite Element Methods*. Marcel Dekker Ltd, New York (USA), 2003.

[14] De Gersem H., Gyselinck J., Dular P., Hameyer K., Weiland T.: "Comparison of Sliding Surface and Moving Band Techniques in Frequency-Domain Finite Element Models of Rotating Machines". *Proceedings of the 6th International Workshop on Electric and Magnetic Fields, EMF*, Aachen (Germany), 2003.

[15] De Gersem H., Weiland T.: "Harmonic Weighting Functions at the Sliding Surface Interface of a Finite Element Machine Model Incorporating Angular Displacement". *IEEE Transactions on Magnetics*, Vol. 40, No. 2, March 2004.

[16] Eilenberger A., Schmidt E., Schrödl M.: "Sensorless Capability of Permanent Magnet Synchronous Machines due to Saturation- and Reluctance-Based Coupling Effects". *Proceedings of the 1st IEEE International Symposium on Sensorless Control for Electrical Drives, SLED*, Padova (Italy), 2010.